HIGH-FIDELITY AERODYNAMIC LOADS ANALYSIS OF THE DOUBLE-SWEPT ERATO ROTOR AT HIGH TRHUST FORWARD FLIGHT OPERATING POINT

Mikel Balmaseda Aguirre
DAAA/ONERA
Institut Polytechnique de Paris
Meudon, France

Hyeonsoo Yeo
U.S. Army Combat Capabilities Development
Command Aviation & Missile Center
Ames Research Center, Moffet Field, CA, USA

François Richez
DAAA/ONERA
Institut Polytechnique de Paris
Meudon, France

Rohit Jain
U.S. Army Combat Capabilities Development
Command Aviation & Missile Center
Ames Research Center, Moffet Field, CA, USA

ABSTRACT

The validity of using comprehensive analysis (CA) tools coupled with computational fluid dynamics (CFD) to predict the aerodynamics of classical rotor blades was proven in the literature. This paper aims to enhance this validation for the complex double-swept planform ERATO blade under high-thrust level-flight condition. In order to do so, RCAS and HOST comprehensive analysis tools and Helios/RCAS and elsA/HOST high-fidelity loose couplings are compared to the results of the experimental campaign of the ERATO blade that was carried out by ONERA in 1998 at the S1MA transonic wind tunnel. Trim commands, airloads and pressure coefficient distribution are used to validate the numerical simulations. The results highlight the need for high-fidelity methods in order to accurately predict the aerodynamic response. The numerical data provided by the high-fidelity methods are used to analyse the flow features that are at the origin of the airloads variations.

NOTATION

A	rotor disk area, πR^2
a	speed of sound, m/s
c	chord, m
C_L	rotor lift coefficient, $L/\rho(\Omega R^2)A$
C_p	pressure coefficient
C_X	rotor propulsive force coefficient, $X/\rho(\Omega R^2)A$
f_m	blade section pitching moment per unit length, N
f_n	blade section normal force moment per unit length, N/m
L	rotor lift, N
M^2c_n	blade section normal force coefficient, $f_n/\frac{1}{2}\rho a^2 c$
M^2c_m	blade section pitching moment coefficient, $f_m/\frac{1}{2}\rho a^2 c^2$
P	rotor power, kW
R	blade radius, m
r/R	relative span
X	rotor propulsive force, N
x/c	normalised chord-wise coorinate
α_s	shaft angle (positive for rearward tilt), deg
β_{1c}, β_{1s}	longitudinal and lateral flapping, deg
θ_0	collective, deg
θ_{1c}, θ_{1s}	lateral and longitudinal cyclic, deg
μ	advance ratio
ρ	freestream density, kg/m^3
σ	rotor solidity
Ω	rotor angular velocity, rad/s

INTRODUCTION

Aero-elastic simulations of helicopter rotor using high-fidelity methods based on CFD (Computational Fluid Dynamics) were developed and implemented over the last decades. The growth of the computational resources allowed for improvements of this numerical approach leading to an accurate representation of the complex aerodynamic phenomena encountered around helicopter rotors. Based on high quality data of flight and wind-tunnel tests, the numerical simulations have been successfully validated for the full-scale UH-60A rotor

(Refs. 1–3) and the model-scale 7A and 7AD rotors in forward flight (Refs. 4–7). These publications showed that airloads and structural loads can be predicted with satisfactory agreement. However, for nonclassical blade-shapes like the double-swept ERATO blade (Étude d'un Rotor Aéroacoustique Technologiquement Optimisé) the existing literature is limited (Refs. 8–11). In 1998 the ERATO blade was tested at S1MA transonic wind tunnel at ONERA's Modane-Avrieux center as shown in Figure 1. Despite the extensive experiments of the ERATO rotor, few validations of the existing aeromechanical tools were performed previously (Refs. 10–12).

Figure 1: ERATO setup in ONERA's S1MA wind tunnel.

The high-speed and the high-advance-ratio flight conditions were largely studied in the past years with the development of the RACER, Airbus Helicopters' high-speed compound helicopter demonstrator (Refs. 13–15) and the RAIDER, Sikorsky's co-axial rotor helicopter (Refs. 16, 17).

The high thrust condition in level flight was studied in (Ref. 7) highlighting the relationship between blade-vortex interaction (BVI) and the dynamic stall observed on the retreating blade (both for lift and pitching moment) at a moderate advance ratio ($\mu = 0.3$). For higher advance ratio cases, the dynamic stall on the retreating blade is present, but does not seem to be induced by a BVI (Ref. 18).

Most of the previous studies were dedicated to simple blade geometries with constant chord and a tip region with a small sweep angle. For more complex blade geometries, especially with a double-swept planform, the aeroelastic phenomena can be more complex and the validity of the simulation tools is not guaranteed. Therefore, this article aims to analyse the double-swept planform ERATO blade at high-thrust condition in forward-flight in order to highlight the physical phenomena and the validity of the proposed methods.

This activity is conducted in the framework of the United States/France Project Agreement on Rotatory Wing Aeromechanics and Human Factors Integration Research agreement. The U.S. Army Combat Capabilities Development Command Aviation & Missile Center (DEVCOM AvMC) and ONERA, The French Aerospace Lab, investigate the airloads and structural loads of the ERATO rotor. The objective is to assess the accuracy of the prediction of ERATO rotor blade loads at various operating points.

This work is focused on the aerodynamic analysis of the ERATO rotor using standalone comprehensive analysis (CA) and high-fidelity coupled CFD/CA at high-thrust level-flight ($\mu = 0.313$, $C_L/\sigma = 0.09675$ and $C_X/\sigma = 0.00494$) as a complement to the high-advance-ratio operating point presented previously in (Refs. 10, 11).

METHODS

The analytical results were obtained using both standalone comprehensive analyses and coupled CFD/CA analyses. ONERA used elsA (Ref. 19) for CFD and HOST (Ref. 20) for CA, and the U.S. Army used Helios (Ref. 21) for CFD and RCAS (Refs. 22, 23) for CA. Descriptions of each analysis and how they are coupled to produce a higher fidelity solution are provided in this section.

elsA

The elsA CFD code (Ref. 19), developed at ONERA, solves the unsteady Reynolds-Averaged Navier-Stokes (URANS) equations for both background Cartesian grids and blade curvilinear grids. Cartesian grid generation and overset grid assembly is done automatically by the pre- and post-processing tool Cassiopee (Ref. 24). The spatial discretization of the equations is performed with Jameson's cell-centered second order scheme, using 2nd and 4th order coefficients of artificial viscosity. The unsteady algorithm corresponds to a backward Euler scheme, with an implicit Gear scheme for the 2nd-order time integration. The time step is equivalent to 0.25 degrees. The non-linear problem is solved iteratively with 30 Newton sub-iterations. Turbulence is taken into account by the Kok $k-\omega$ (Ref. 25) model, with Menter shear stress transport (SST) corrections (Ref. 26) and Zheng limiter (Ref. 27). The flow is modeled as fully turbulent. The near-body grids of the blades are rotated and deformed following the blade motion and trim provided, through the loose partitioned coupling, by the rotorcraft comprehensive analysis HOST.

HOST

HOST (Helicopter Overall Simulation Tool) (Ref. 20) is a rotorcraft comprehensive analysis developed by Airbus Helicopters. HOST modeling of blade dynamics is multibody-like. The blade is represented as an assembly of rigid segments connected by virtual joints. Euler-beam modeling provides 3 degrees of freedom (flapwise bending, chordwise bending, and torsion). A modal reduction approach is used to reduce the number of degrees of freedom from a large system of equations. The aerodynamics of HOST uses a lifting line approach based on airfoil look-up tables combined with a wake model. In this effort, among the several wake models available, a prescribed wake helical geometry was used. For the coupling with elsA, HOST airloads are corrected, via the delta method (Ref. 1), by the CFD airloads.

The ERATO rotor blade is modeled in HOST using 34 rigid elements connected by virtual hinges (flap, lag, and torsion). Blade dynamic responses are calculated with eight modes and eight harmonics. Section lift, drag, and moment values for the airfoils are obtained from airfoil look-up tables. For the current study, both HOST and RCAS used the C81Gen generated airfoil tables computed by the U.S. Army. C81Gen is a Navier-Stokes based program that generates an airfoil table in C81 format. C81Gen runs two-dimensional, time-dependent compressible solver ARC2D with structured body fitted viscous gridding. A 5.0 deg azimuthal step size was used for the structural dynamics and trim calculations in HOST.

Helios

Helios (HELIcopter Overset Simulations) (Ref. 21), developed by the U.S. Army and the Department of Defense Computational Research and Engineering Acquisition Tools and Environments - Air Vehicles (CREATE^{TM}-AV) program, is a multidisciplinary computational platform for high-fidelity rotorcraft analysis. Helios uses a multi-mesh, multi-solver paradigm. Near-body solvers such as NASA's OVERFLOW (Ref. 28) structured solver and FUN3D (Ref. 29) unstructured solver, kCFD unstructured solver (Ref. 30), and mStrand multi-strand solver (Ref. 31) are integrated in Helios to capture the wall-bounded viscous effects. Cartesian grids in the off-body are used to resolve the wake through a combination of higher-order algorithms and adaptive mesh refinement (AMR). The Cartesian off-body grids are solved with SAMCart using a 5th-order central difference scheme in space and either a 3rd-order explicit 3-stage Runge-Kutta scheme or 2nd-order implicit lower-upper symmetric-Gauss-Seidel method (LU-SGS) BDF2 in time. An overset procedure facilitates data exchange and also enables relative motion between meshes using the parallel domain connectivity solver PUNDIT (Parallel UNsteady Domain Information Transfer). Helios also has the ability to perform CFD/CA coupling using the comprehensive analysis codes RCAS and CAMRAD II (Ref. 32) which allows the blades to be trimmed throughout the course of these simulations.

In this effort Helios solves the near-body grids around the rotor blades and test stand with the CFD solver OVERFLOW, using a 5th-order central difference scheme in space and a 2nd-order backward differentiation formula (BDF2) scheme in time. The turbulent flow is modeled using the Langtry-Menter transitional shear stress transport (SST-LM-G) turbulence model in both the near- and off-body grids. The time step is equivalent to an azimuthal step size of 0.25 deg. AMR was not used.

RCAS

Rotorcraft Comprehensive Analysis System (RCAS) (Refs. 22, 23) is a comprehensive analysis developed by the U.S. Army to provide state-of-the-art rotorcraft modeling and analysis technology for Government, industry, and academia. It is a multi-disciplinary software system capable of detailed modeling a wide range of rotorcraft configurations operating in hover, forward flight, and maneuvering flight to predict performance, loads, vibration, flight dynamics, and aeroelastic stability.

The ERATO rotor blade is modeled in RCAS using 18 nonlinear beam elements and 28 aerodynamic segments. As mentioned, both HOST and RCAS use the same airfoil tables generated by the U.S. Army. The rotor hub was modeled as fully articulated with pitch bearing and flap and lag hinges. The elastomeric lag damper of the ERATO rotor was modeled with equivalent hinge stiffness and damping values at the lag hinge. A 5.0 deg (72 steps per rotor revolution) azimuthal step size was used for the structural dynamic calculations in RCAS. The RCAS standalone analysis was conducted using nonuniform inflow with prescribed wake geometry and unsteady aerodynamics based on classical quasi-steady Theodorsen theory (Ref. 33).

CFD/CA coupled analysis

The CFD/CA coupling procedure used the standard partitioned loose or "delta" coupling approach (Ref. 1). At each coupling iteration the aerodynamic loads calculated by CFD are passed to CA. After trimming with the CFD airloads, CA computes the blade deflections and passes them back to CFD. This sequence is repeated until the airloads, deflections, and control angles converge. The trim parameters used in the predictions are the same as those from the test, a four degree-of-freedom trim. The trim targets are the specified rotor lift, rotor propulsive force and zero first harmonic flapping.

Both elsA and Helios CFD codes use overlapping grids consisting of structured curvilinear near-body grids rotating in a Cartesian background grid. Helios/RCAS uses a turbulent model that accounts for the laminar-to-turbulent transition while elsA/HOST models a fully turbulent flow.

The computational grids model the ERATO rotor blade geometry and test stand, but do not include a hub or the wind tunnel walls.

The size of the elsA grid shown in Figure 2.a is approximately 32.7M points: 5.5M points for blade body-fitted grids, 1M points for test stand, and 26.2M points for Octree background grid. The minimal grid size of the background mesh is approximately 9% of the main chord (0.14 m).

For Helios, shown in Figure 2.b, fully structured overset solver OVERFLOW was used for the ERATO blades. Each blade grid has approximately 26M nodes and the stand grid has approximately 2.9M nodes. In the off-body, 8 levels of grid are used with fixed refinement regions around the blade and test stand with a total of 234M nodes. For these regions, the finest grid spacing is approximately 6% of the tip chord.

In the HOST and elsA/HOST analyses, the blade is represented by the first eight eigenmodes and the blade periodic response was calculated with up to eight harmonics. For the

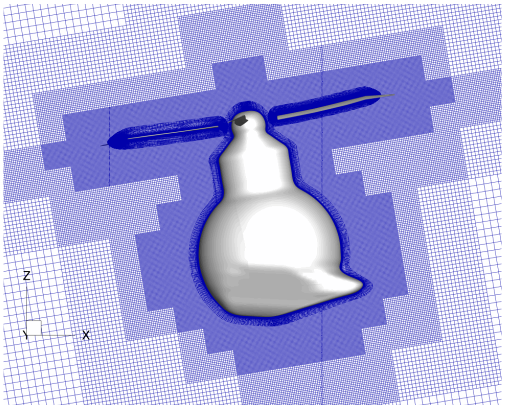

(a) elsA mesh.

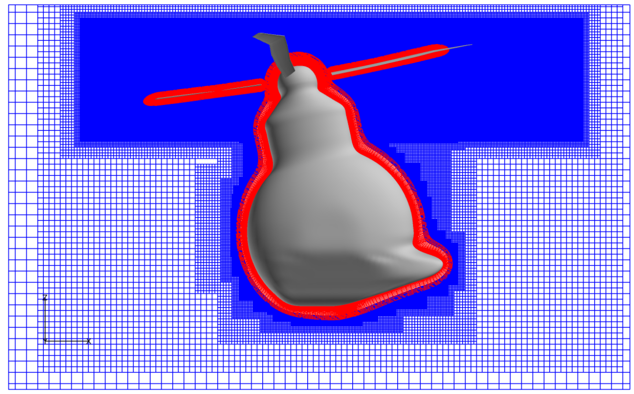

(b) Helios mesh.

Figure 2: Overset meshes used for the CFD analyses.

RCAS and Helios/RCAS analyses, full finite element representation of the blade is maintained throughout the dynamic analysis and no harmonic truncation is used. Neither comprehensive analysis included blade structural damping, test stand dynamics, or drive train dynamics. Previous study showed that test stand and drivetrain dynamics for this test apparatus did not appear to play a significant role for rotor loads correlation (Ref. 5).

NUMERICAL ANALYSIS

In this work the double-swept ERATO rotor is studied under a high-thrust level flight at moderate advance-ratio ($\mu = 0.313$) condition. The ERATO rotor is a four-bladed fully articulated rotor, with a radius of 2.1 m and solidity, σ, of 0.085. The ERATO rotor blades have an aero-acoustically optimized design conceived by the DLR and ONERA in the 90s (Refs. 9,12,34,35). One of the particularities of the blade is that it has a double-swept planform as shown in Figure 3. The linear twist rate is -10 deg/R. The blade is equipped with airfoils from the OA family. The OA312 airfoil is used up to 70% of the blade radius. Then the airfoil transitions to OA409 at 90% and to OA407 at the blade tip. A large set of flight conditions were studied in various experimental campaigns in 1998. The level-flight tests (used as a reference in this paper) were carried out at ONERA's S1MA wind tunnel in the Modane-Avrieux center located in the French Alps, the hover tests were performed in Marignane by Eurocopter (currently Airbus Helicopters) and the aero-acoustic campaign took place at the DNW wind tunnel in Netherlands.

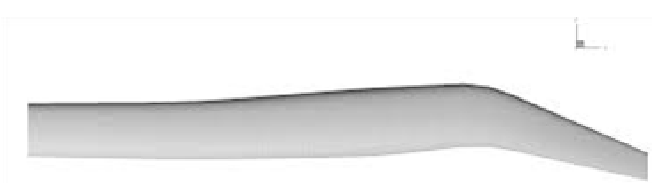

Figure 3: Planform of the ERATO blade.

A moderate advance-ratio at high-thrust experimental point was chosen for this study ($\mu = 0.313$, $M_{Tip} = 0.618$, $C_L/\sigma = 0.09675$ and $C_x/\sigma = 0.000505$). Four degrees of freedom (dof) trim was carried out with the rotor thrust, propulsive force and zero flappling ($\beta_{1c} = \beta_{1s} = 0$) as objectives and controlled by the commands of the collective pitch angle, cyclic pitch angles (θ_0, θ_{1c} and θ_{1s} respectively) and the shaft angle (α_s).

The remainder of this section highlights two different aspects of the studied analysis. First, the capabilities of the proposed numerical tools are validated for the studied complex ERATO rotor emphasizing the difference between the rapid and the high-fidelity coupling tools. This study is carried out through a trim and power analysis and an airloads study at the specific sections of the blade where the experimental data are available. Second, a deeper study on the physical aspects of the high-thrust flight is presented.

Trim and power analysis

The converged values for trim commands and the rotor power are shown in Table 1. All the proposed methods provide a good prediction for the commands with respect to the experimental trim except for the θ_{1c} angle where the minimum relative error percent is provided by the elsA/HOST coupling (13%). Ortun et al. (Ref. 4) observed this phenomenon and highlighted that the test-stand has a non-negligible effect on the θ_{1c} angle. Thus, the important deviation ($> 38\%$) of the comprehensive tools (HOST and RCAS) with respect to the experimental results and the significant improvement of the high-fidelity couplings (Helios/RCAS and elsA/HOST) prediction is expected. This is due to the upwash (front side) and downwash (rear side) effect created by the test-stand which is not modelled by the comprehensive tools. About 1 deg error in the prediction of θ_{1c} is observed with the high-fidelity tools, however, a similar deviation was obtained for the previously performed 7A rotor analyses and the ERATO analyses at high advance ratio (Ref. 4).

As observed with the convergence of the commands, the power prediction is improved with the high-fidelity aerodynamics couplings. RCAS and Helios/RCAS provide a better

Table 1: Command and power values at convergence.

	θ_0 (deg)	θ_{1c} (deg)	θ_{1s} (deg)	α_s (deg)	P (kW)
Test	9.80	4.70	-3.91	-6.84	60.03
RCAS	8.23	2.31	-3.58	-7.36	63.11
HOST	9.20	2.02	-3.57	-6.91	71.3
Helios/RCAS	9.23	3.86	-4.07	-6.98	62.22
elsA/HOST	9.60	4.10	-3.86	-7.21	68.48

agreement than HOST and elsA/HOST. This result is difficult to interpret due to several reasons: differences in trim control angles, differences in blade deformation or differences in the turbulence model and the numerical methods could impact the power prediction. Nevertheless, CFD codes tend to overestimate the power due to the fully turbulent modelling, used by elsA, which tends to overestimate the friction force and, thus, the blade profile drag power. The Helios/RCAS power prediction takes into account laminar-to-turbulent transition of the boundary layers improving the predictions of the couplings with high-fidelity aerodynamics as in (Ref. 36).

Airloads

The section normal force (M^2c_n) and the section pitching moment (M^2c_m) are studied and compared to the experimental results at five different radial sections, corresponding to the 0.5, 0.75, 0.85, 0.925 and 0.975 relative-span (r/R), in order to validate the prediction of the comprehensive and high-fidelity tools. In the remainder of the article the same color and style of these graphs are considered. Thus, the experimental results are plotted with a solid black line, the comprehensive analyses are shown with dashed lines while the high-fidelity results are solid lines, the results of the US Army are plotted in blue and the results of ONERA are green.

Figures 4a to 4e show the M^2c_n load as a function of the azimuth at five radial positions. The normal force coefficient (c_n) of the high-fidelity couplings is obtained by integrating the pressure coefficient (C_p) of the blade skin at the positions where the experimental Kulites are located. The magnitude of the M^2c_n response increases when the studied section approached the tip of the blade.

The section located at 50% of the blade span (Figure 4a) presents an increased lift from 0 deg of azimuth until 170 deg of azimuth. Then, the lift drops up to the minimum M^2c_n value observed at 270 deg of azimuth. The overall response of the studied methods is accurate and represents the waveform of the experimental response both in terms of amplitude and phase. The comprehensive analyses (RCAS and HOST) provide a significant overestimation of the response in the neighborhood of 0 deg azimuth. The coupled Helios/RCAS and elsA/HOST models improve the accuracy of the prediction.

The remaining sections, shown in Figures 4b to 4e, present a double minimum peak of the M^2c_n at 80 deg (weak amplitude) and at 120 deg (strong amplitude) of azimuth. HOST is capable of reproducing the double-peak dynamic but does not model the amplitudes accurately. RCAS analyses show that the first peak has the largest amplitude, inverting the experimental trend. In terms of amplitude, RCAS results overestimate the magnitude of the minimum peaks. The location of the minimum peak computed by both comprehensive analy-

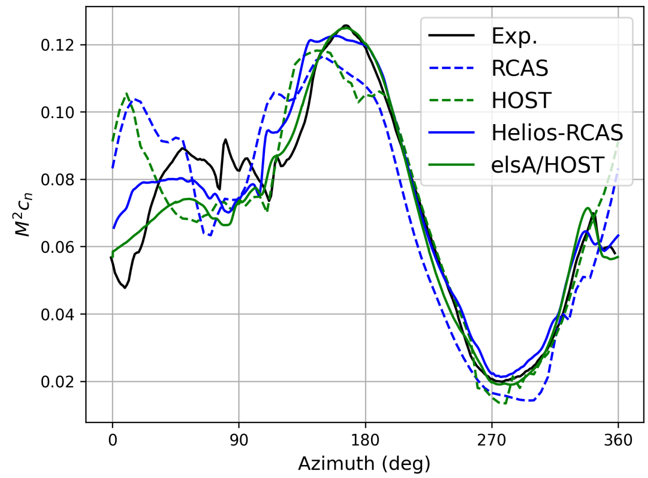

(a) Radial position: r/R= 0.5.

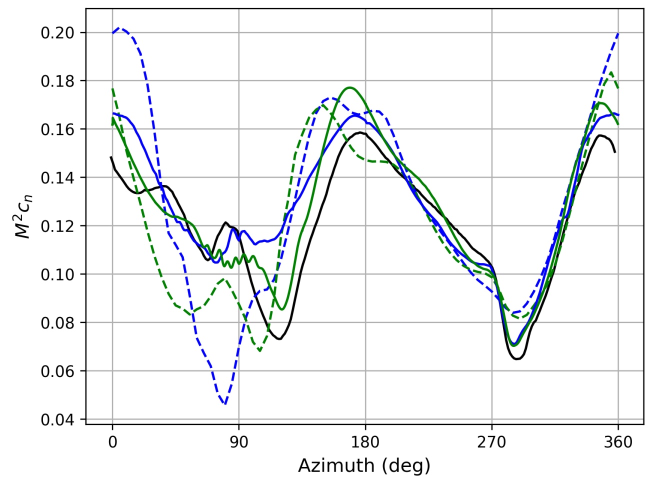

(b) Radial position: r/R= 0.75.

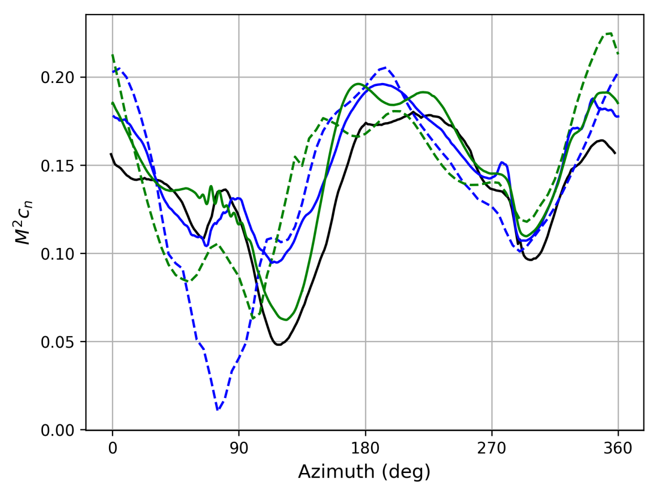

(c) Radial position: r/R= 0.85.

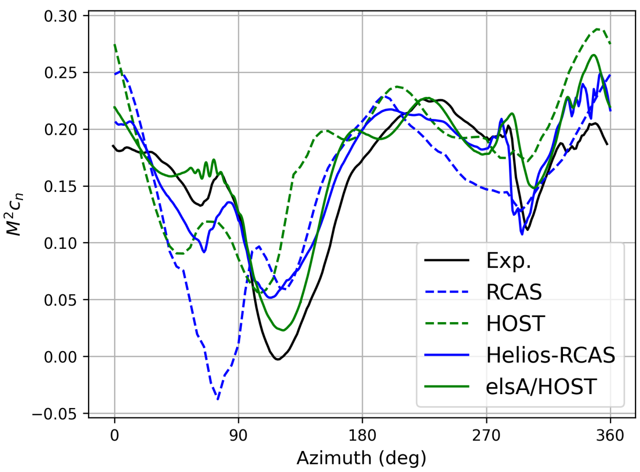

(d) Radial position: r/R= 0.925.

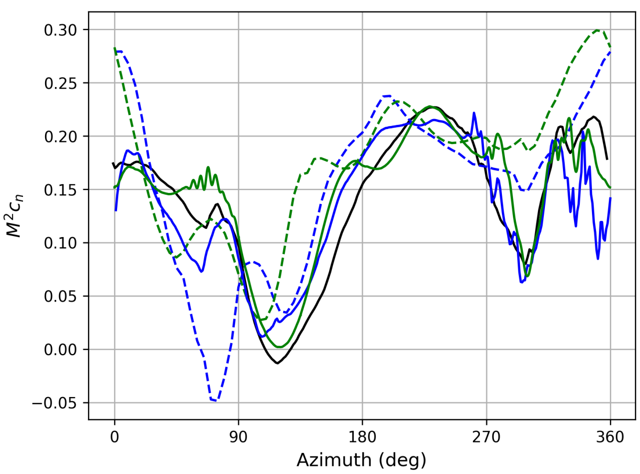

(e) Radial position: r/R= 0.975.

Figure 4: M^2c_n graphs at different radial positions.

sis codes is mismatched with respect to the experimental results. The latter, is a known phenomenon induced due to the time-lag-effect of the transonic flow, missing on the 2D airfoil tables used by the comprehensive codes. Despite the lift reduction, all the radial positions present a positive value of the M^2c_n. This effect is amplified through the span attaining a zero M^2c_n value at the tip section. The high-fidelity CFD/CA couplings are capable of capturing this effect and matching the azimuthal position for the minimum lift. Helios/RCAS seems to underpredict the amplitude of the lift-drop on the advancing blade while elsA/HOST provides a better representation with a slight underestimation of the M^2c_n amplitude.

The experimental data has a peak of the M^2c_n in the neighborhood of 180 deg of azimuth. The transition from this value to the minimum value observed between 270 deg and 300 deg is different with the studied section: a) at 50% and 75% of the blade span, the lift reduction follows a linear slope; b) the remaining sections, present an initial lift stagnation and then the M^2c_n value drop abruptly.

Between 270 deg and 300 deg of azimuth, the experimental lift slightly increases before reaching a minimum peak of M^2c_n. The location of the increase/reduction of M^2c_n, is shifts from 280 deg azimuth (at 70% of the blade span) to 300 deg azimuth (at 85% and 92.5% of the blade azimuth) showing a radial translation of this phenomenon. The tip section is stalled from 270 deg.

All the numerical analyses reproduce the M^2c_n reduction trend between 180 deg and 270 deg of azimuth. However, the M^2c_n stall is not reproduced by the comprehensive codes. The coupled analyses significantly improve the correlation with the experimental data. The M^2c_n increase and drop effect in terms of amplitude and phase is correctly reproduced by Helios/RCAS and elsA/HOST. After the blade vortex interaction, between azimuth 300 deg and 360 deg, the coupled models tend to overestimate the lift recovery between 75% and 85% of the blade span. However, the tip stall recovery is underestimated by Helios/RCAS.

The M^2c_m moment is studied as a function of the azimuth in Figures 5a to 5e for the same radial positions as the M^2c_n.

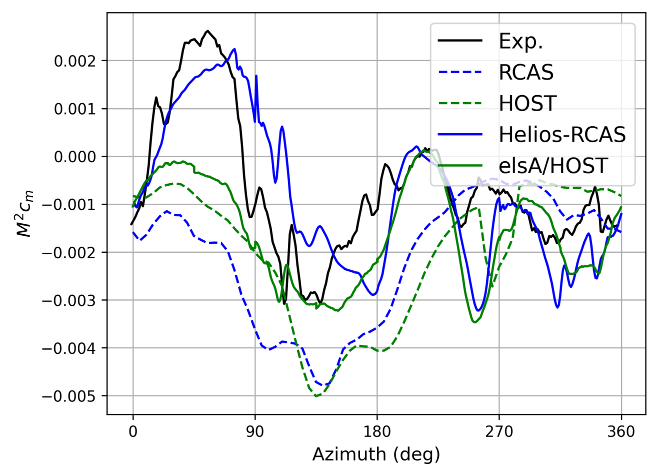

(a) Radial position: r/R= 0.5.

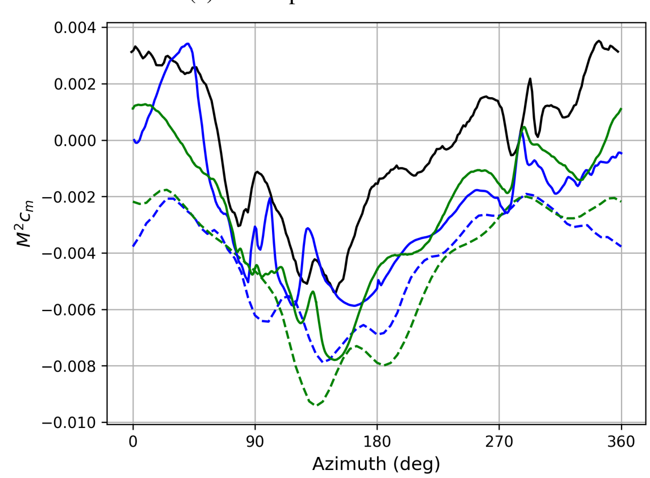

(b) Radial position: r/R= 0.75.

Similarly, the M^2c_m maximum and minimum values increase as the radial position approaches the outer regions of the blade.

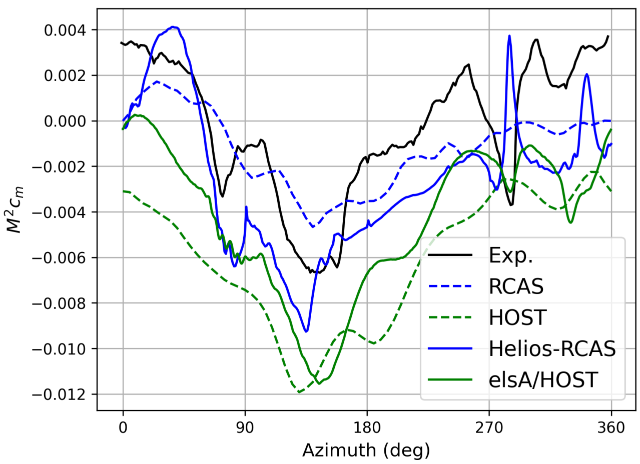

(c) Radial position: r/R= 0.85.

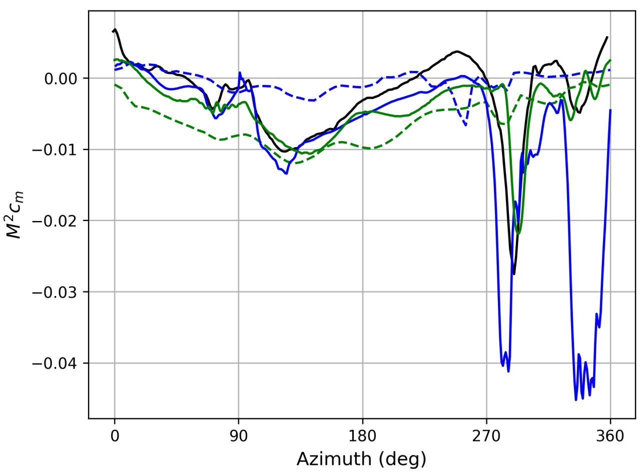

(d) Radial position: r/R= 0.925.

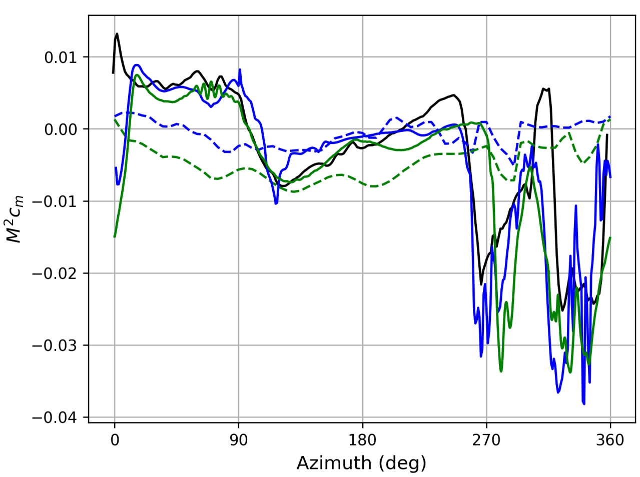

(e) Radial position: r/R= 0.975.

Figure 5: M^2c_m graphs at different radial positions.

The section located at 50% of the blade span (Figure 5a) presents a positive peak of M^2c_m at 45 deg of azimuth. Then, the pitching moment is reduced until 120 deg of azimuth. Then the experimental data show some oscillations around a value M^2c_m of ≈ -0.0015. The correlation of the numerical analyses is reduced compared to the one of the M^2c_n airload. At this location, Helios/RCAS provides good approximative results.

The remaining sections, shown in Figures 5b to 5e, observe a flattened response of the M^2c_m between 0 deg and 90 deg of azimuth. Then, the M^2c_m drops until a local minimum peak of negative value at 120 deg of azimuth. Between 120 deg of azimuth and the location of the stall occurrence on the retreating blade, the M^2c_m increases linearly. Then, at the sections between 75% and 85% of the blade span a M^2c_m increase and drop effect occurs. At the outer sections, 92.5% and 97.5% of the blade span, a double pitching moment stall is observed. The first moment stall event occurs between 270 and 300 deg of azimuth. The second one is weaker and occurs between 330 and 360 deg.

The comprehensive codes are not capable of reproducing the pitching moment stall observed at the outer sections. The overall shape of M^2c_m is captured, however, the magnitude is underestimated. The coupled high-fidelity analyses significantly improve the correlation with respect to the experimental data. Both Helios/RCAS and elsA/HOST are capable of reproducing the shape and level of the M^2c_m between 20 deg and 270 deg of azimuth. The double dynamic stall at the tip section is accurately predicted. However, at 92.5% of the blade span, Helios/RCAS predicts a second M^2c_m stall that is as strong as the first one, while it is hardly visible in the experimental results. However, at 97.5% of the blade span, the two stall events, that are clearly visible in the experiments, present similar amplitude, and are well captured by both Helios/RCAS and elsA/HOST.

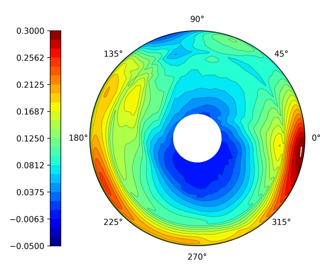

(a) HOST.

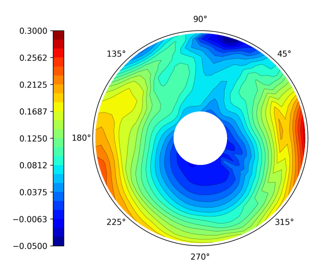

(b) RCAS.

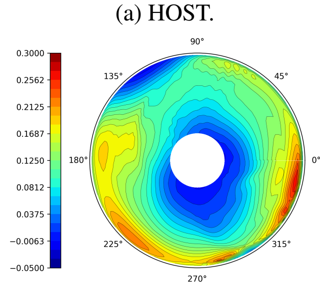

(c) elsA/HOST.

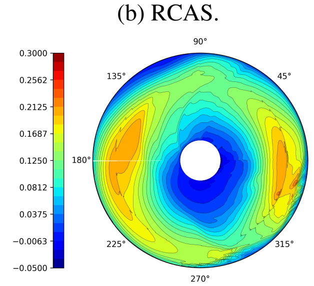

(d) Helios/RCAS.

Figure 6: M^2c_n rotor map.

Figures 6 and 7 show respectively the M^2c_n and M^2c_m rotor map of the numerical analyses without considering the Kulites integration. As discussed previously, the transonic effect induces a delay on the azimuthal position of the negative lift on the tip of the advancing blade. The CA tools predict the negative lift on the tip of the blade in the neighborhood of 90 deg. In terms of magnitude, RCAS seems to perform better than HOST which underestimates the minimum lift value. RCAS presents a large negative lift region prior to the 90 deg of azimuth. Similarly, CA tools seem to overestimate the positive lift region between 180 deg and 225 deg of azimuth and 0 deg while elsA/HOST coupling seems to have an extended maximum lift region but with smaller magnitude. The M^2c_m rotor map shows larger variations with the high-fidelity CFD/CA analyses, specially at the blade tip. On the retreating blade, between 270 deg and 300 deg of azimuth where the dynamic stall appears, the high fidelity CFD/CA predict a positive moment on the blade root and a negative moment effect on the blade tip. The root moment is slightly captured by the CA tools. As studied previously, the dynamic stall of the M^2c_m occurs in two phases.

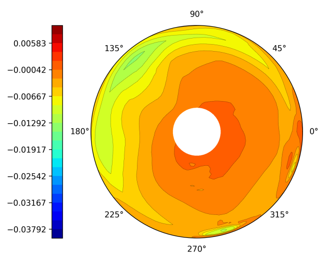

(a) HOST.

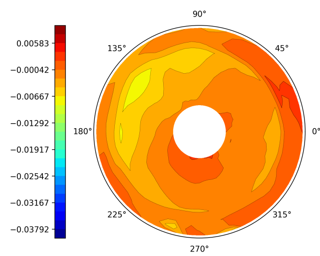

(b) RCAS.

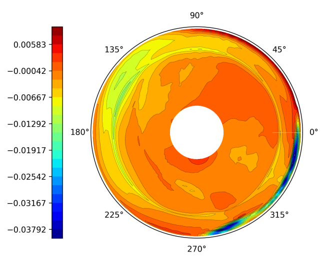

(c) elsA/HOST.

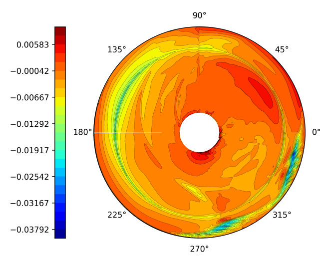

(d) Helios/RCAS.

Figure 7: M^2c_m rotor map.

The origin of the observed dynamic stall in the retreating blade is investigated in the following sections.

Wake analysis

The results presented in the previous section highlighted the need to better understand the origin of the dynamic stall observed in the retreating blade. Different authors in literature have identified that Blade-Vortex-Interaction (BVI) could trigger the dynamic stall on the retreating blade (Ref. 7), especially for an advance-ratio of 0.3, close to the value of the present study. At higher advance-ratio and for non-conventional blade-shapes, the role of the rotor wake in stall triggering is not clear. Furthermore, the advancing blade side is also a potential region of BVI that could impact the evolution of the airloads. This section aims to identify the interaction between the wakes and the blades on the retreating side.

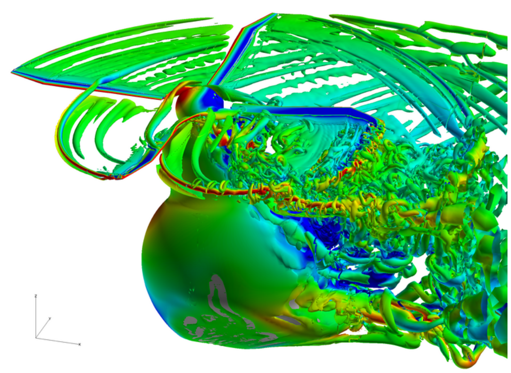

(a) Helios/RCAS.

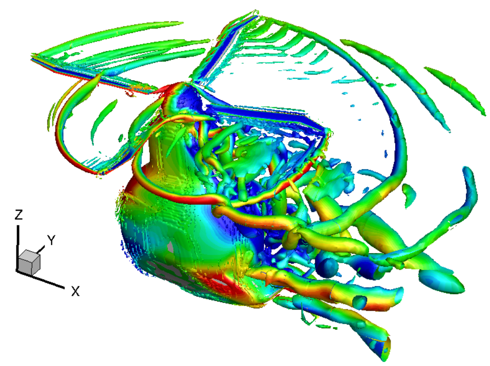

(b) elsA/HOST.

Figure 8: Isocontours of Q-criterion, wake representation of the ERATO rotor.

Figure 8 shows an overview of the wake of the ERATO rotor from the high fidelity coupled analyses with the iso-Qcriterion colored by the vorticity magnitude in order to observe the wake of all the blades and the test stand when the retreating blade is located at 280 deg of azimuth. A BVI is observed on the retreating blade at around 70% of the blade span. The tip vortex of the retreating blade, interacts with the inner region of the blade located at 180 deg of azimuth and the advancing blade, presenting a double BVI.

Both Helios/RCAS and elsA/HOST provide similar wake results. The wake structures with Helios seem to be more discretized due to a higher order resolution on the background mesh. The trajectory of the wakes and the effect of wake fainting on the advancing blade (due to the lift that approaches zero value) is also present at similar locations.

The retreating blade between azimuths 270 deg and 300 deg shows a dynamic stall triggered by a BVI and affects both the lift and the pitching moment airloads. The BVI is present at 70% of the radius when the blade is located at 280 deg of azimuth and shifts radially towards the tip at 300 deg of azimuth. Figure 9 highlights the BVI computed by Helios/RCAS and elsA/HOST. The isoQ-criterion is represented to observe the wake interaction radial shift. Two different slices are carried out representing the vertical velocity field. The first slice is performed at the location of the TE of the retreating blade at 280 deg. Then, in order to highlight the influence of the BVI,

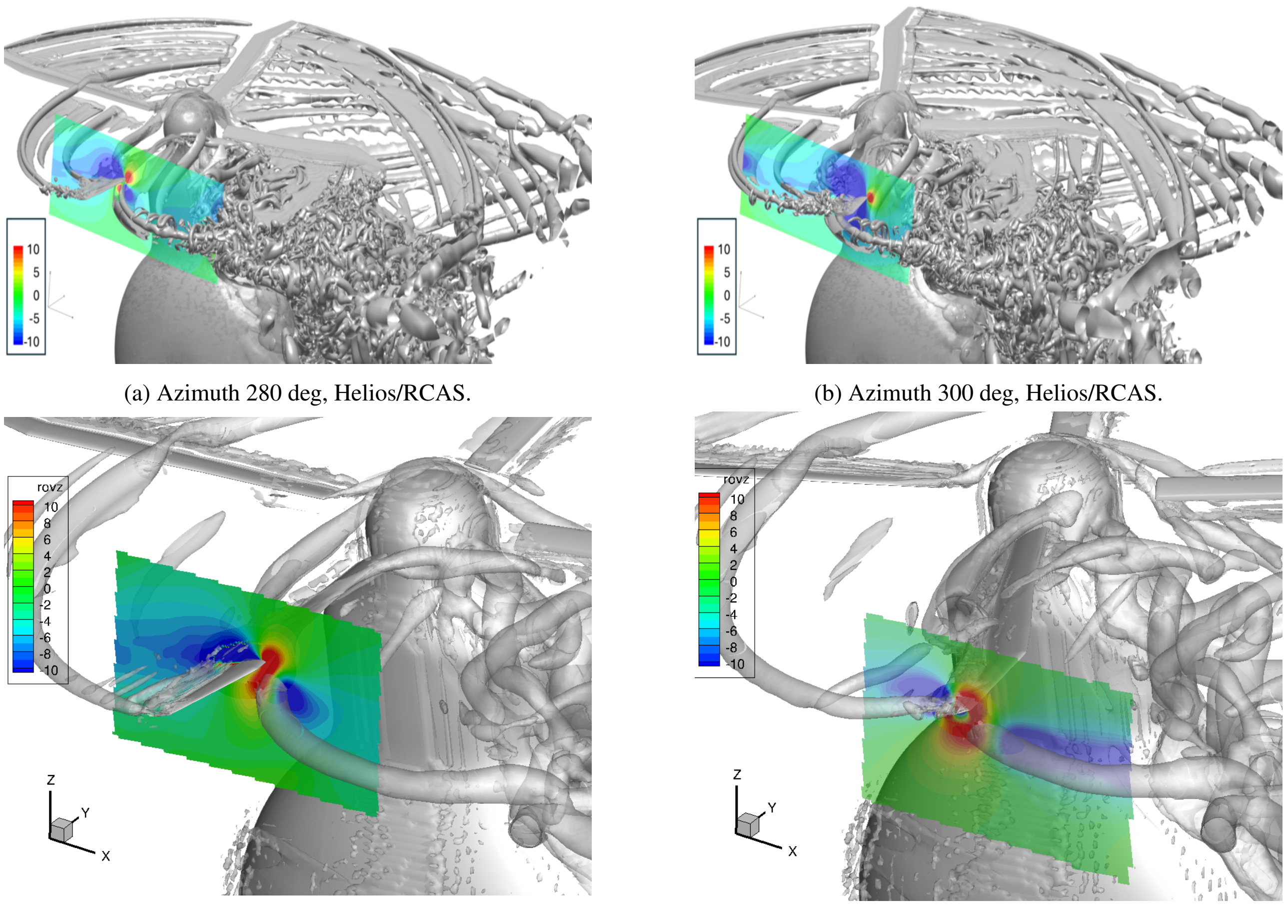

(a) Azimuth 280 deg, Helios/RCAS.

(b) Azimuth 300 deg, Helios/RCAS.

(c) Azimuth 280 deg, elsA/HOST.

(d) Azimuth 300 deg, elsA/HOST.

Figure 9: Analysis of the wake interaction, vertical velocity slices.

a second slice is performed on each of the radial interaction sections (≈70% at 280 deg of azimuth and ≈97.5% at 300 deg of azimuth). These figures show that the BVI is strong and that the upwash effect of the wake triggers the first phase of the dynamic stall.

Both Helios/RCAS and elsA/HOST analyses show a similar primary wake distribution on the retreating blade. elsA/HOST results present a larger numerical diffusion and the secondary wakes observed in the Helios/RCAS anlysis are dissipated. The latter could be due to the use by Helios/RCAS of higher-order schemes in the background mesh, which allows for a better representation of the wake.

Chord-wise aerodynamics of the blade tip

This section aims to validate the chord-wise prediction of the loads computed by the CFD/CA couplings and to study the behavior of the outer sections where the experimental data is available. Figure 10 shows the pressure coefficient C_p with respect to the normalized chord-wise coordinate (x/c) where 0 corresponds to the leading-edge (LE) and 1 to the trailing-edge (TE).

Six azimuthal positions (0.4 deg, 90 deg, 120 deg, 180 deg, 270 deg and 300 deg) where the experimental data was available are studied using the high-fidelity CFD/CA results for the two tip sections (92.5% and 97.5% of the blade span). Overall, the numerical predictions are capable of accurately capturing the various phenomena that take place over the blade.

The experimental results in Figures 10a and 10d show that the blade at 0.4 deg is operating nominally. A maximum absolute values of Cp is observed both for the pressure and the suction sides close to the LE of the blade, as the flow remains attached. At 92.5% of the blade span both Helios/RCAS and elsA/HOST provide accurate results and the C_p distribution is representative of the experimental results. However, both numerical models provide a stalled configuration. Thus, the lift recovery at the blade tip is not represented.

The experimental results at 90 deg seem to present a plateau that could imply the existence of a bubble with a large suction peak in the suction side at $\approx 0.2x/c$ position. Helios/RCAS results, using the Langtry-Menter turbulence model, predict a laminar boundary layer until the location of the shock, then, the pressure gradient triggers the transition. The modeling presents an effective delay allowing for the boundary layer to re-attach. This behavior could be representative of a small laminar separation bubble induced by the shock. The differ-

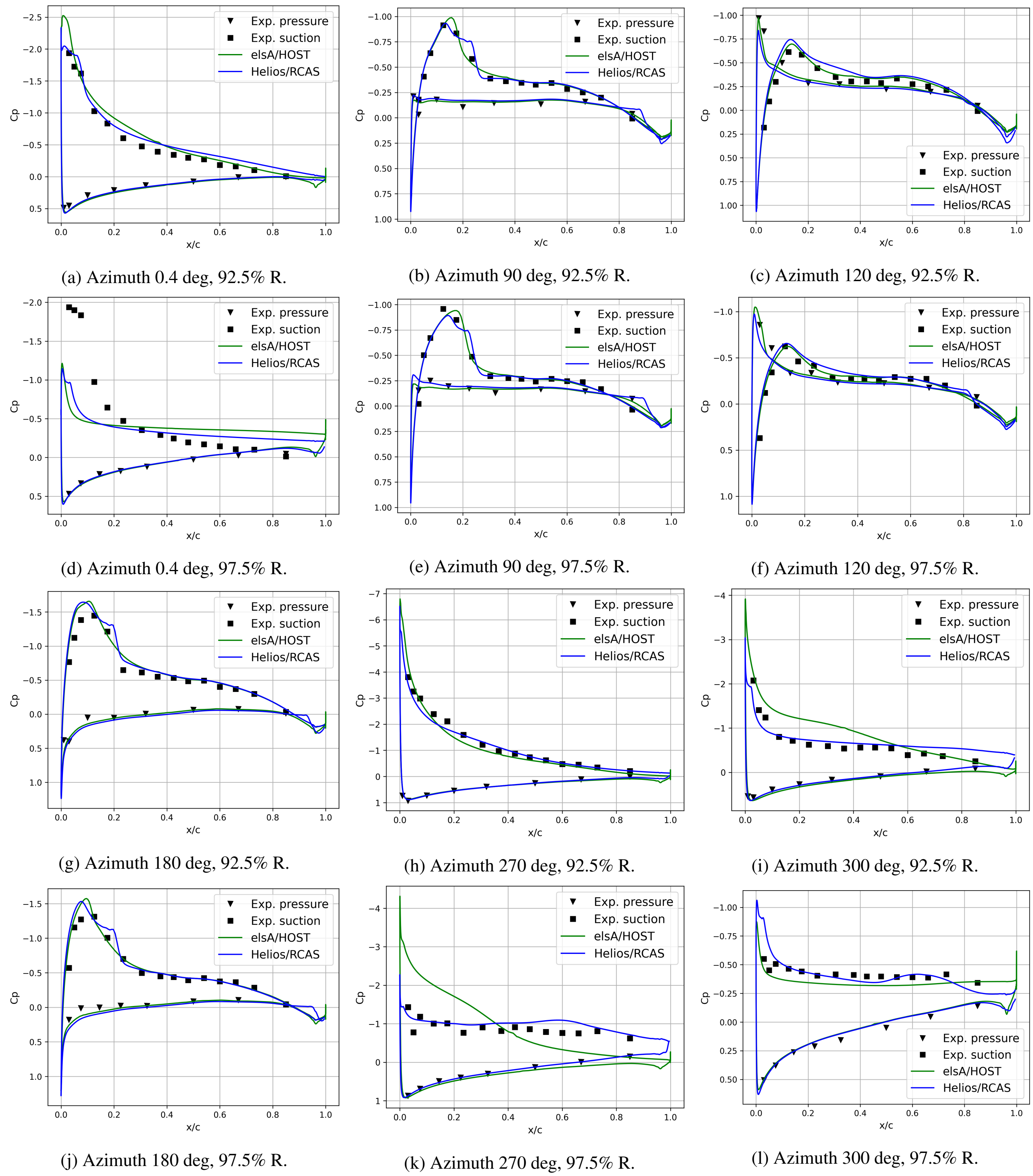

(a) Azimuth 0.4 deg, 92.5% R.

(b) Azimuth 90 deg, 92.5% R.

(c) Azimuth 120 deg, 92.5% R.

(d) Azimuth 0.4 deg, 97.5% R.

(e) Azimuth 90 deg, 97.5% R.

(f) Azimuth 120 deg, 97.5% R.

(g) Azimuth 180 deg, 92.5% R.

(h) Azimuth 270 deg, 92.5% R.

(i) Azimuth 300 deg, 92.5% R.

(j) Azimuth 180 deg, 97.5% R.

(k) Azimuth 270 deg, 97.5% R.

(l) Azimuth 300 deg, 97.5% R.

Figure 10: C_p distribution at different radial locations.

ence of the elsA/HOST results could be due to the full turbulence modelling. The numerical predictions are representative of the C_p distribution measured by the experiment. The experimental results lay between Helios/RCAS and elsA/HOST results being difficult to identify the observed phenomenon with the existing Kulites position. While the blade advances on its azimuthal position, at 120 deg, the sonic shock or the pre-bubble state of the suction side is diffused with a large suction effect at the LE of the pressure side.

As shown in Figures 10g and 10j, at 180 deg, the blade behaves close to the condition described at 90 deg azimuth.

The peak of the suction side is spread between the LE and $\approx 0.25x/c$ location. Then, a lift drop is observed consequence of a shock or a pre-bubble and the lift value stagnates. The pressure side, behaves nominally for a low incidence profile. Helios/RCAS and elsA/HOST provide similar predictions and are representative of the experimental data.

Figure 10h corresponds to the retreating blade at the 92.5% of the blade span, the profile behaves nominally like a profile under large angle of attack where the lift center is close to the LE. Both Helios/RCAS and elsA/HOST provide an accurate prediction. Figure 10k present the rotor tip at 270 deg of azimuth. Both the experimental data and Helios/RCAS analysis present a stalled profile where the lift is significantly reduced at the suction side and is flattened through the chord. elsA/HOST analysis predicts a profile that has not yet reached stall.

At 300 deg azimuth, Figures 10i and 10l, a pitching-moment-dynamic-stall behavior is present with a lift-stall. The lift is significantly reduced, specially at the tip section. The lift center shifts towards the TE inducing the observed negative pitching moment airload. Both Helios/RCAS and elsA/HOST are capable of reproducing the stalled phenomenon accurately.

SUMMARY AND CONCLUSIONS

This article presents the aerodynamic loads analysis of the double-swept ERATO rotor under high-thrust level-flight condition. This work was developed in the framework of the United States/France Project Agreement on Rotatory Wing Aeromechanics and Human Factors Integration Research. Different CA and CFD/CA tools are presented and compared (RCAS, Helios/RCAS, HOST and elsA/HOST). The trim and airloads are compared to the experimental data. An special attention is taken to the wake interactions and the in-chord behavior of the blade aerodynamics. From this study, the following conclusions are obtained:

- Comprehensive analyses tend to underpredict blade pitch angles. Coupled analyses, which include the test-stand modeling, increase blade pitch angles and improve overall correlation. Especially, improvement of lateral cyclic angle correlation is notable.

- The rotor blade aerodynamic environment at high thrust is characterized by several blade vortex interactions that trigger a dynamic stall in the retreating blade. The latter takes place in two different steps: the first, consists in a lift and pitching moment stall, then, the second step shows a pitching-moment dynamic-stall, however, the lift does not stall.

- For the normal force comparison, the standalone comprehensive analyses show reasonably good correlation on magnitude, but the phase correlation is poor. This is due to the limitations of the 2D airfoil tables. The coupled analyses significantly improve the phase of the lift reduction and waveform in the first quadrant. The pitching moment on the advancing side and the pitching-moment dynamic-stall on the retreating side are also better captured by the coupled analyses than the comprehensive analyses based on lifting-line aerodynamics.

- On the advancing blade side, the high-fidelity simulations show that the lift reduction at the tip approaching a zero value lead to a dissapearence of the tip vortex.

- The high-thrust at 0.31 advance-ratio level-flight condition implies that the retreating blade interact with the wake of the previous blades. Furthermore, the wake of the retreating blade interacts with the following blades.

- The high-fidelity couplings are capable of capturing the pressure distribution on the chordwise direction accurately.

- The high-fidelity coupling simulations show that the blade interaction induces a dynamic stall in two steps. The BVI modifies its radial position when the azimuth increases shifting towards the tip of the blade.

REFERENCES

1. Mark Potsdam, Hyeonsoo Yeo, and Wayne Johnson. Rotor airloads prediction using loose aerodynamic/structural coupling. *Journal of Aircraft*, 43(3):732–742, 2006.

2. Hyeonsoo Yeo and Mark Potsdam. Rotor structural loads analysis using coupled computational fluid dynamics/computational structural dynamics. *Journal of Aircraft*, 53(1):87–105, 2016.

3. François Richez, Rohit Jain, Marilyn Smith, Amanda Grubb, and Camille Castells. Validation and analysis of aeroelastic simulations of the uh-60a rotor from pre- to post-stall flight conditions. In *76th Annual Forum & Technology Display (Vertical Flight Society)*, 2020.

4. Biel Ortun, Mark Potsdam, Hyeonsoo Yeo, and Khiem Van Truong. Rotor loads prediction on the onera 7a rotor using loose fluid/structure coupling. *Journal of the American Helicopter Society*, 62(3):1–13, 2017.

5. Hyeonsoo Yeo, Mark Potsdam, Biel Ortun, and Khiem Van Truong. High-fidelity structural loads analysis of the onera 7a rotor. *Journal of Aircraft*, 54(5):1825–1839, 2017.

6. François Richez. Analysis of dynamic stall mechanisms in helicopter rotor environment. *Journal of the American Helicopter Society*, 63(2):1–11, 2018.

7. Camille Castells, François Richez, and Michel Costes. A numerical analysis of the dynamic stall mechanisms on a helicopter rotor from light to deep stall. *Journal of the American Helicopter Society*, 65(3):1–17, 2020.

8. Biel Ortun, Didier Petot, Khiem-Van Truong, and Roger Ohayon. Towards a new generation of rotorcraft comprehensive analysis; coupling with csm and cfd. 2008.

9. Philippe Beaumier, Berend G van Der Wall, Kurt Pengel, Christoph Kessler, Marc Gervais, Yves Delrieux, Jean-François Hirsch, and Pascal Crozier. From ERATO basic research to the blue edgetm Blue Edge™ rotor blade: an example of virtual engineering? In *Rotorcraft Virtual Engineering Conference*, 2016.

10. Mikel Balmaseda Aguirre, Hyeonsoo Yeo, Buvana Jayaraman, and Biel Ortun. High-fidelity aerodynamic loads analysis of the double-swept erato rotor. In *50th European Rotorcraft Forum, Marseille, France*, September 10-12, 2024.

11. Hyeonsoo Yeo, Mikel Aguirre Balmaseda, Buvana Jayaraman, François Richez, and Biel Ortun. High-fidelity structural loads analysis of the double-swept erato rotor. In *50th European Rotorcraft Forum, Marseille, France*, September 10-12, 2024.

12. Y Delrieux, J Prieur, M Costes, P Gardarein, P Beaumier, H Mercier des Rochettes, P Leconte, P Crozier, WR Splettstoesser, B Van der Wall, et al. The onera-dlr aeroacoustic rotor optimisation programme erato: methodology and achievements. In *American Helicopter Society Aerodynamics, Acoustics and Test and Evaluation Technical Specialists Meeting, San Francisco*, 2002.

13. Felix Frey, Jakob Thiemeier, Constantin Öhrle, Manuel Keßler, and Ewald Krämer. Aerodynamic interactions on airbus helicopters' compound helicopter racer in cruise flight. *Journal of the American Helicopter Society*, 65(4):1–14, 2020.

14. Boisard Ronan. Time efficient methodology for the evaluation of aerodynamics and flight mechanics of the racer compound helicopter in hover under cross wind conditions. In *VFS 68-Forum 68-The Vertical Flight Society*, 2022.

15. Constantin Öhrle, Felix Frey, Jakob Thiemeier, Manuel Keßler, and Ewald Kräamer. Coupled and trimmed aerodynamic and aeroacoustic simulations for airbus helicopters' compound helicopter racer. *Journal of the American Helicopter Society*, 64(3):1–14, 2019.

16. Jinggen Zhao, Mikel Brigley, Ramin Modarres, and William A Welsh. S-97 raider rotor vibratory loads analysis using cfd-csd. In *AIAA SciTech 2019 Forum*, page 0860, 2019.

17. Yanqin Zhao, Ye Yuan, and Renliang Chen. Optimal transition of coaxial compound helicopter after total propeller failure. *Journal of Aerospace Engineering*, 37(6):04024086, 2024.

18. Camille Castells, François Richez, and Michel Costes. A numerical investigation of the influence of the blade–vortex interaction on the dynamic stall onset. *Journal of the american helicopter society*, 66(3):1–13, 2021.

19. L Cambier, M Gazaix, S Heib, S Plot, M Poinot, JP Veuillot, JF Boussuge, and M Montagnac. An overview of the multi-purpose elsa flow solver. *Aerospace Lab*, (2):p–1, 2011.

20. Bernard Benoit, Konstantin Kampa, W von Grunhagen, Pierre-Marie Basset, and Bernard Gimonet. Host, a general helicopter simulation tool for germany and france. In *Annual Forum Proceedings-American Helicopter Society*, volume 56, pages 1110–1131. American Helicopter Society, INC, 2000.

21. Andrew M Wissink, Dylan Jude, Buvaneswari Jayaraman, Beatrice Roget, Vinod K Lakshminarayan, Jayanarayanan Sitaraman, Andrew C Bauer, James R Forsythe, and Robert D Trigg. New capabilities in CREATE™-av helios version 11. In *AIAA Scitech 2021 Forum*, page 0235, 2021.

22. Hossein Saberi, Matthew Hasbun, J Hong, Hyeonsoo Yeo, and Robert A Ormiston. Overview of rcas capabilities, validations, and rotorcraft applications. In *American Helicopter Society 71st Annual Forum, Virginia Beach, VA*, 2015.

23. Matthew Hasbun, Hossein Saberi, and Hyeonsoo Yeo. Overview of rcas capabilities and validations for rotorcraft and evtol applications. In *Vertical Flight Society 80th Annual Forum & Technology Display, Montreal, Canada*, 2024.

24. Christophe Benoit, Stéphanie Péron, and Sâm Landier. Cassiopee: a cfd pre-and post-processing tool. *Aerospace Science and Technology*, 45:272–283, 2015.

25. J. C. Kok. Resolving the dependence on freestream values for the k-ω turbulence model. *AIAA Journal*, 38:1292–1295, July 2000.

26. Manikandan Ramasamy, Rohit Jain, and Thomas R Norman. Data-driven analysis of cycle-to-cycle variations, scatter, and furcation in the uh-60a wind tunnel rotor airloads measurements. *Journal of the American Helicopter Society*, 67(4):1–21, 2022.

27. X Zheng, C Liao, C Liu, CH Sung, and TT Huang. Multigrid computation of incompressible flows using two-equation turbulence models: Part i—numerical method. 1997.

28. RH Nichols and PG Buning. Overfow user's manual, version 2.2. *NASA Langley Research Center, Hampton, VA*, 2010.

29. Robert T Biedron, Jan-Reneé Carlson, Joseph M Derlaga, Peter A Gnoffo, Dana P Hammond, Kevin E Jacobson, William T Jones, Bil Kleb, Elizabeth M Lee-Rausch, Eric J Nielsen, et al. Fun3d manual: 13.7. Technical report, 2020.

30. David R McDaniel, Todd Tuckey, and Scott A Morton. The hpcmp CREATE^{TM}-av kestrel computational environment and its relation to nasa's cfd vision 2030. In *55th AIAA Aerospace Sciences Meeting*, page 0813, 2017.

31. Jayanarayanan Sitaraman, Vinod K Lakshminarayan, Beatrice Roget, and Andrew M Wissink. Progress in strand mesh generation and domain connectivity for dual-mesh cfd simulations. In *55th AIAA Aerospace Sciences Meeting*, page 0288, 2017.

32. Wayne Johnson. Technology drivers in the development of camrad ii. In *American helicopter society aeromechanics specialists conference, San Francisco, California*, pages 3–1, 1994.

33. Theodore Theodorsen. General theory of aerodynamic instability and the mechanism of flutter. Technical report, 1979.

34. Jean Prieur and Wolf R Splettstoesser. Erato-an onera-dlr cooperative programme on aeroacoustic rotor optimization. 1999.

35. WR Splettstoesser, BG van der Wall, B Junker, K-J Schultz, P Beaumier, Y Delrieux, P Leconte, and P Crozier. The erato programme: wind tunnel test results and proof of design for an aeroacoustically optimised rotor. 1999.

36. Rohit Jain. Computational fluid dynamics transition models validation for rotors in unsteady flow conditions. *Journal of Aircraft*, 59(4):875–895, 2022.